J Mater Sci (2007) 42:8771–8787
DOI 10.1007/s10853-007-1719-2

Superelasticity, energy dissipation and strain hardening of vimentin coiled-coil intermediate filaments: atomistic and continuum studies

Theodor Ackbarow · Markus J. Buehler

Received: 3 January 2007 / Accepted: 23 March 2007 / Published online: 10 July 2007

Abstract Vimentin coiled-coil alpha-helical dimers are elementary protein building blocks of intermediate filaments, an important component of the cell's cytoskeleton that has been shown to control the large-deformation behavior of eukaryotic cells. Here we use a combination of atomistic simulation and continuum theory to model tensile and bending deformation of single alpha-helices as well as coiled-coil double helices of the 2B segment of the vimentin dimer. We find that vimentin dimers can be extended to tensile strains up to 100% at forces below 50 pN, until strain hardening sets in with rapidly rising forces, approaching 8 nN at 200% strain. We systematically explore the differences between single alpha-helical structures and coiled-coil superhelical structures. Based on atomistic simulation, we discover a transition in deformation mechanism under varying pulling rates, resulting in different strength criteria for the unfolding force. Based on an extension of Bell's theory that describes the dependence of the mechanical unfolding force on the pulling rate, we develop a fully atomistically informed continuum model of the mechanical properties of vimentin coiled-coils that is capable of predicting its nanomechanical behavior over a wide range of deformation rates that include experimental conditions. This model enables us to describe the mechanics of cyclic stretching experiments, suggesting a hysteresis in the force–strain response, leading to energy dissipation as the protein undergoes repeated tensile loading. We find that the dissipated energy increases continuously with increasing pulling rate. Our atomistic and continuum results help to interpret experimental studies that have provided evidence for the significnificance of vimentin intermediate filaments for the large-deformation regime of eukaryotic cells. We conclude that vimentin dimers are superelastic, highly dissipative protein assemblies.

T. Ackbarow · M. J. Buehler (✉)
Laboratory for Atomistic and Molecular Mechanics, Department of Civil and Environmental Engineering, Massachusetts Institute of Technology, Cambridge, MA 02139, USA
e-mail: mbuehler@MIT.EDU

Introduction: the structure of vimentin intermediate filaments and role in eukaryotic cells

Together with beta sheets, alpha helical (AH) structures are the most abundant secondary structures found in proteins. These two patterns are particularly common because they result from hydrogen bonding between the N–H and C=O groups in the polypeptide backbone. An alpha helix is generated when a single polypeptide chain twists around on itself stabilized by hydrogen bonds (H-bond) made between every fourth residue, linking the O of peptide i to the N of peptide $i + 4$ in the residue chain. Consequently, at each convolution, three H-bonds are found in parallel arrangement that stabilize the helical configuration [1].

Another particularly stable configuration, found for the first time in keratin intermediate filaments (IFs) about 50 years ago, are alpha helical coiled-coils, where the primary structure reveals a pronounced seven residue periodicity $(abcdefg)_n$, called a heptad repeat. Within this repeat, positions ''a'' and ''d'' are preferably occupied with nonpolar residues [2] such as LEU, ALA, VAL or ILE. The hydrophobic residues—consequently concentrated on one side—are the reason for the coiled-coil structure. In order to avoid contact with surrounding water molecules, AHs assemble into coiled-coils by wrapping

around each other and clustering the hydrophobic side chains inside [1]. Additionally, interhelical and intrahelical salt bridges contribute to coiled-coil thermodynamic stability and are expected to enhance resistance to mechanical stretch in a nonstereospecific manner [3].

Coiled-coils are also the building blocks of vimentin intermediate filament (IF) dimers, which are composed of a head, a tail, and an extremely elongated central rod-domain. A schematic of the vimentin dimer structure is shown in Fig. 1a. The rod-like structure is 310 residues long and consists of four coiled-coil alpha helices (1A, 1B, 2A, 2B) divided by linkers (L1, L12, L2) [2, 4, 5, 7, 8]. Interestingly, all helices in the rod domain have different lengths.

The lengths of each of the components are absolutely conserved for all types of IFs in different types of cells. Additionally, either ends of the rod as well as the position of the stutter in the 2B segment are highly conserved (a definition of various biological terms and concepts is provided in Table 1) [2, 4, 5, 9]. The stutter is an irregularity in the periodic sequence, where four extra residues are inserted into the continuous heptad repeat, what results in an almost parallel run of both helices without interrupting the coiled-coil geometry. For all types of IFs, the stutter is spaced precisely six heptads away from the C-terminal end of coil 2B [4]. In contrast to the conserved regions, the head and tail domain are greatly diverse for all types of IFs [2, 4].

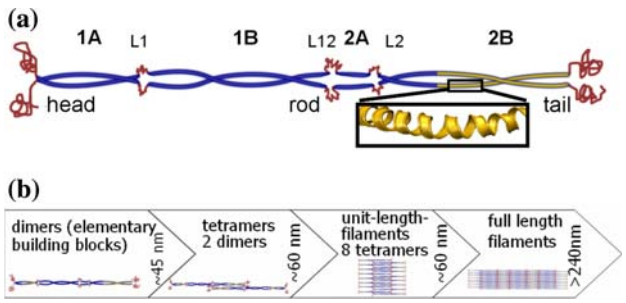

Fig. 1 Geometry of vimentin intermediate filament, from atomistic to macromolecular structure. Subplot (**a**): The dimers, approximately 45 nm long, are the elementary building blocks of vimentin intermediate filaments. A dimer consists of a head, tail (plotted in red) and an elongated rod domain which is divided into four alpha-helical coiled coils (1A, 1B, 2A, 2B) connected through linkers L1, L12, L2 (also red) [2]. The molecular dynamics simulations described in this paper are performed on alpha-helices, placed in the 2B segment (yellow). Subplot (**b**): Intermediate filaments assembly hierarchically into fibrils. Dimers, the elementary building blocks, assembly through a half-staggered, anti-parallel overlap into tetramers, which associate laterally into 13 nm thick unit-length-filaments (ULFs). In the next step, ULFs assembly longitudinally into more compact filaments (10 nm in diameter) with a length of more than 240 nm [2, 4–6]

The five types of IFs and the three assembly groups are listed in Table 2. The most widely distributed of all IF proteins is vimentin, typically expressed in leukocytes, blood vessel endothelial cells, some epithelial cells, and mesenchymal cells such as fibroblasts [1].

The role of IF networks in the cytoskeleton

IFs, in addition to microtubules (MTs) and microfilaments (MFs) are one of the three major components of the cytoskeleton in eukaryotic cells [11]. The cytoskeleton plays a critical role in determining the shape and the mechanical properties of the cell, and is vital for numerous additional functions such as cell motility or protein synthesis [11–13].

Like many other biological materials, IFs are hierarchical structures with highly specific features at nanoscale. Vimentin IF dimers, shown schematically in Fig. 1a, are the elementary building blocks of IFs and thus represent the first level of hierarchy. Through following the different steps of assembly (Fig. 1b) [14, 15], dimers associate to fibrils, which build the second level of hierarchy. In vivo, these fibers can reach a length of up to several μm and consist of 16 dimers in cross-section. The third level of hierarchy are three-dimensional IF-networks inside the cell, reinforcing the plasma membrane [4, 12, 16]. Inside the network, IF-associated proteins such as plectins generate the connection between individual filaments.

The cell's IF networks are connected with other cells' networks and with the extracellular matrix at the plasma membrane [1]. This architecture guarantees that tensile and shear loads applied to the tissue can be carried by IF networks.

The fact that IFs span from the cell nucleus to the cell membrane, and interact with IF networks of other cells suggest that IFs play an important role in transmitting mechanical signals from the plasma membrane to the nucleus, where a specific response can be triggered by mechanical stimulation [10, 17].

Plakin-type cross-bridging proteins, also known as cytolinkers (e.g. plectins or desmoplakins) link all three cytoskeletal networks (MTs, MFs and IFs). These proteins attach the IFs to MTs, MFs or adhesion complexes [18]. However, to date little is known about these interaction or the mechanical functions of plakin-proteins and their ability to store or/and dissipate any elastic energy during internal contraction or external deformation [2, 11].

In contrast to MTs and MFs, IFs do not participate in the dynamic functions of the cytoskeleton. Further, they do not support active transport of motor proteins such as myosin and kinsesin, due to the missing polarity in the protein structure (in contrast to MT and MF networks) [2]. They do not participate in any cell movement [1]. These evidences

Table 1 Summary of different biological terms and concepts used in this paper

Cytoskeleton:	A composite inside the cell consisting of three different networks: Actin filaments, microtubules and intermediate filaments. The intermediate filament network is in the focus of this paper. These networks connect the nucleus (nuclear membrane) with the plasma membrane and are furthermore responsible for the organization inside the cell.
Intermediate filaments (IFs):	One of the three components of the cytoskeleton; mainly responsible for the large deformation behavior of the cell.
Cross bridging proteins:	Cross bridging proteins form connections inside each cytoskeletal network as well as connections between different networks.
Dimer:	A dimer is the elementary building block of an IF fiber. This protein consists of a head domain, a tail domain and an extremely elongated coiled-coil rod. A coiled-coil is a superhelix that consists of two alpha helices that twist around each other.
Assembly:	Individual IF dimers assemble systematically and hierarchically into filaments (Fig. 1b). Two dimers build a tetramer, two tetramers build an octamer and four octamers build a unit length filament (ULF). Once this level of assembly is reached, ULFs ally longitudinally into long fibers.
Residue:	The primary structure of a protein consists of a sequence of amino acids. One residue is thus one amino acid in the polypeptide backbone.
Conserved structure:	A structure is conserved when parts of the residue sequence are similar or do not very at all between the different species (e.g. human and fish). For example, certain parts of the IF sequence are very similar between different species as well as inside the IF protein family (vimentin, desmin, keratin, etc.). Conserved structures often signify a particular amino acid sequence that has proven to be particularly suitable for a specific task, and has thus been kept identical during the evolutionary process.

Table 2 Different types of intermediate filaments, its location in the cell and its assembly group. Intermediate filaments are classified into five different types. Most of them appear in the cytoskeleton, except lamins that are found in the nucleoskeleton. Keratins, in contrast to the other IF types, assemble into heterodimers, consisting of one acidit and one basic keratin [6, 10]

#	Type	Location	Assembly group
I.	Acidic keratins	Cytoskeleton	AG I (heterodimer)
II.	Basic keratins	Cytoskeleton	AG I (heterodimer)
III.	Vimentin, desmin	Cytoskeleton	AG II (homodimer)
IV.	Neurofilaments	Cytoskeleton	AG II (homodimer)
V.	Lamins	Nucleoskeleton	AG III (homodimer)
VI.	Phakinin, filesin	Eye lens cells	

underline the specific static-mechanical role of IFs. These static-mechanical properties are the focus of the work described in this paper.

Mechanical properties of IFs compared to other cytoskeletal components

A great diversity of mechanical properties enables the vimentin IFs to satisfy their specific mechanical role in cells, such as to guarantee their structural integrity or their shape. It has been hypothesized that IFs are critical to provide strength to the cell under large deformation, and to absorb large amounts of energy upon a certain load by unfolding [19, 20]. This represents a means to reinforce the cell in extreme deformations so that cells can withstand dramatic loads and deformations [11, 19, 20].

IFs exhibit a highly nonlinear stress–strain relationship with a high resistance against rupture, also known as strain hardening. Figure 2 depicts experimental results [7] of the stress–strain response of gels composed of the three cytoskeletal proteins. In these rheological experiments, gels with equal weight concentrations were sheared and the deformation response (strain) was measured. It is apparent that vimentin gels are capable of sustaining large deformation at large forces. In contrast, actin filaments rupture at low strains but large forces, and MTs break at moderately large strains, but small forces. This underlines the significance of vimentin IFs to carry large forces at large deformation.

The stiff behavior of MTs and MFs may be one reason for much smaller breaking strains of approximately 60% for MT and 20% for MF in networks of equal weight concentration (see Fig. 2) [7]. In contrast, IFs feature much higher extensibility. It has been suggested that a higher flexibility of IFs at small strains (compared with MFs) results in a lower mechanical resistance during cell movement, mainly performed by MFs. It has also been shown that the rigidity of circulating lymphocytes and fibroblasts primary depends on vimentin IFs, whereas MTs play a minor role [11, 21–23]. The different mechanical properties of the cytoskeletal networks clearly indicate that the cytoskeleton is a composite with a range of mechanical

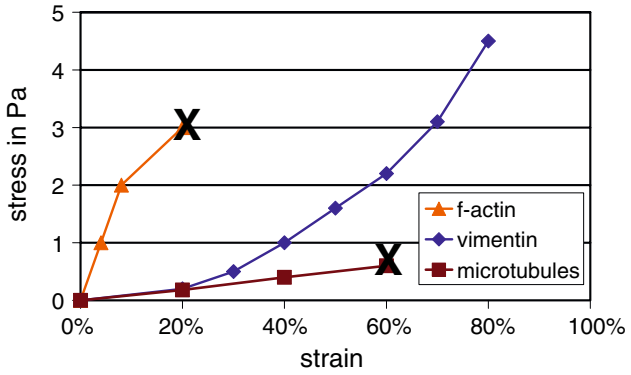

Fig. 2 Shearing experiments carried out with gels of equal weight concentration demonstrate the differences in the mechanical properties of various cytoskeletal networks. In contrast to vimentin that sustains strains much larger than 80%, MT break at 60% strain, and MF break at 20% strain. Additionally, vimentin gels exhibits continuous significant strain hardening. We note that this stress strain curve is different from the behavior of a single protein as reported in this paper due to the different level of hierarchy. *Data source:* Janmey et al. [7]

properties, which cannot be achieved by a polymer network composed out of a single type of polymer.

Further, experiments have revealed that the mechanical properties of vimentin determines the cell stiffness in particular for high stress and large deformation [4, 11, 12, 24–26]. For instance, in shear tests vimentin deficient cells were shown to be 40% less stiff at high strains compared with wild-type cells (see Fig. 3), while their elastic properties do not change much under small deformation [11]. These experiments strongly support the notion that the biological significance of vimentin IFs lies in the large-deformation regime.

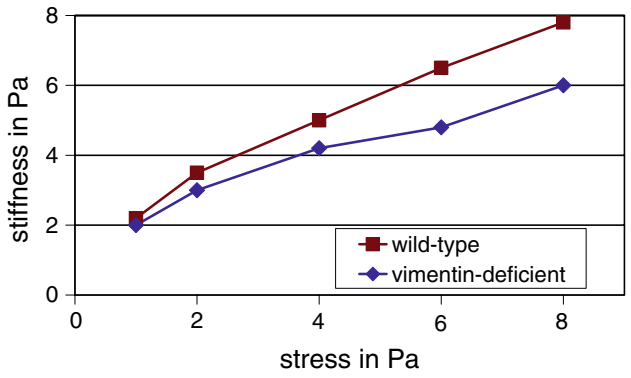

Fig. 3 Stiffness of cells as a function of stress state, comparing wild-type and vimentin deficient cells. It was shown in experiments that vimentin deficient cells are much less stiff at higher stresses than wild-type cells. These results suggest that vimentin proteins play a critical role in particular for the large-deformation elastic properties of cells. It also corroborates the notion that due to the progressive strain hardening at large strains, IFs can be understood as ''security belts'' of the cell that operate after MTs and MFs have ruptured [3]. *Data source:* Wang et al. [11]

Observations in rupture experiments on single IFs have shown a dramatic change in filament diameter, which remained unchanged for hours after rupture appeared [24]. This is a sign for a profound change in the molecular architecture under large deformation. It was suggested that the alpha-helical coiled-coil are converted into beta-sheet-type structures with both strands being aligned along the filament axis. This provided some evidence that the mechanical properties of IFs mainly depend on the nano-mechanical, molecular properties of the coiled-coil dimer [24]. However, no direct experimental, simulation or theoretical prove has been reported thus far.

The parallel assembly of dimers into filaments (see Fig. 1b) may allow for slip between dimers under large deformation. In addition, presence of linkers in the rod domain [26] lead to a higher flexibility of IFs and thus to a smaller bending stiffness and persistence length of the filaments (0.3–1.0 μm) compared to MTs (1–8 mm, due to geometry) and MFs (3–10 μm) [4, 12].

Finally, the mechanical role of intermediate filaments is particularly evident in diseases in which the loss of mechanical function and integrity of various tissues is associated with intermediate-filament-protein mutations [6, 27]. It was shown that mutations in keratin IFs reduce the ability of these IF networks to bundle and to resist large deformation [11]. Furthermore, it has been suggested that point mutations lead to the aggregation of the cytoskeleton and extensive cell fragility in epidermis, heart and skeletal muscle after they are exposed to mechanical strain [28].

Mechanics of similar alpha helical and coiled-coil structures

In recent years, a variety of different alpha-helical structures and coiled-coils were studied in experiment as well as in simulation [28–35].

AFM experiments on single molecules of double-headed myosin, single-headed myosin as well as coiled-coil tail fragments were reported in [29, 31]. It was found that the transition to unfolding of the protein structure (in the following referred to as angular point or unfolding force) begins at strains of about 20% of stretched protein length. Furthermore, it was shown that myosin is a very elastic protein, with almost no hysteresis at small pulling rates. Even if the coiled-coil structure has been unfolded completely under mechanical forces, it refolds again to its initial configuration in less than one second [29]. Some of the characteristics of myosin deformation during tensile tests were also observed in MD simulations that were carried out on parts of the coiled-coil structure [31].

A multi-scale model for human hair that mainly consists of keratin IF coiled-coils was developed in [30]. MD simulations on coiled-coils have shown force-deformation

characteristics similar to the one observed for myosin. Additionally, a pulling rate dependence of the coiled-coil structure was found, and it was suggested that the non-equilibrated system (due to the very high pulling rates in MD) is the reason for this behavior.

Furthermore, some simulations were carried out on single alpha helices [32, 33]. By applying tensile loads, unfolding of the helix was observed after a short steep increase in force. Thereby, the 16 residues long helix in [32] started to unfold at both ends simultaneously, in contrast to the 20-residue long amino acid chain modeled in [33], which unfolded systematically from the side where force was applied.

Research strategy and outline

Experiments on entire cells have provided strong evidence for the importance of mechanical properties of vimentin IFs on the large deformation behavior of cells (see e.g. Figs. 2 and 3). However, it remains unclear if the origin of these effects lies at the molecular protein level, at the level of dimers, or if it is a consequence of larger-scale structural features of the vimentin protein network [4, 24].

Only few alpha-helical structures have been analyzed in experiments or in simulations. Further, until now, neither any systematic studies on the difference between single AHs and coiled-coils were carried out, nor the dependence on the pulling velocity was analyzed in detail. Additionally, no explanations about the highly conserved assembly of AHs into coiled-coils were suggested that consider mechanical aspects. A structure-property link for the three deformation regimes and associated strength models has not been reported. Earlier MD simulations were carried out at extremely large strain rates, and no direct link between simulation and experiment has been reported.

Here we perform a series of atomistic studies of tensile and bending deformation of vimentin to arrive at a detailed understanding of the mechanical behavior of these molecules under small and large deformation and at different pulling velocities. We systematically investigate the pulling rate dependence of the mechanical properties of this particular structure. Development of a theoretical model enables us to develop a rigorous understanding of the pulling rate dependence, which can be used to extrapolate our results to pulling rates that are comparable to those applied in experiment. This leads to a direct link between our simulations and results obtained in experiments. Moreover, the continuum model enables us to predict the behavior of the protein under cyclic loading and under varying pulling rates.

We focus on the coiled-coil structure in the 2B segment of the vimentin rod domain, since this part of the vimentin protein is highly conserved across various species, indicating a significant biological function. The goal is to develop a structure-function relationship on the protein level and to link these properties with biological cellular functions of vimentin.

The outline of the paper is as follows. In 'Theoretical concepts: Modified Bell theory', we present a modification to Bell's classical model that enables us to describe the dependence of protein unfolding forces as a function of pulling rates. In 'Atomistic modeling methods', we briefly introduce our atomistic modeling procedure. In 'Computational results', we report results of atomistic modeling for a variety of boundary conditions. Section 'Atomistically informed continuum model' is dedicated to development of a continuum model, based on the atomistic simulation results reported in 'Computational results'. In the last Sect. 'Discussion and conclusion' we conclude with an extensive discussion of our results in light of biological function and earlier experimental results.

Theoretical concepts: Modified Bell theory

Mechanical loading of protein structures can result in severe changes in the protein structure, inducing unfolding of the protein. Typically, a variety of unfolding processes exist for a given protein structure, each of which has a specific reaction pathway and an associated energy barrier.

The different unfolding modes in the protein can be understood as the interplay between different unfolding processes with different activation barriers operating at different activation distances.

Several theories exist that describe competing processes due to mechanically induced instabilities of protein structures. These concepts stem primarily from the field of physical chemistry [36–40]. Most of them are derived from a theory originally postulated by Bell in 1978 [41].

In Bell's theory, the off rate χ is the product of a natural vibration frequency, ω_0, of the bond in vacuum and the quasi-equilibrium likelihood of reaching the transition state with an energy barrier E_b that is reduced by mechanical energy $f \cdot x_b$, where f is the applied force along the coordinate x, and x_b is the distance between the equilibrated state (minimum of the well) and the transition state.

The off rate, also known from chemical reaction kinetics, is given by

$$\chi = \omega_0 \cdot \exp\left(-\frac{(E_b - f \cdot x_b)}{k_b \cdot T}\right). \quad (1)$$

The off rate describes how often a bond is broken per unit time and equals to the reciprocal of the lifetime of a bond. The natural vibration frequency of a bond is $\omega_0 \approx 1 \times 13\ \mathrm{s}^{-1}$ [41].

However, Eq. 1 does not describe the dependence of the speed at which a bond breaks due to the applied pulling force. Instead, it only provides an estimate of the time scale at which the bond will be broken.

In order to overcome this limitation, we modify Eq. 1 based on the following idea: The speed v at which a bond is broken equals to the distance that needs to be overcome in order to break the bond (x_b) divided by the time for the bond breaking. Consequently, v is the product of $\chi \cdot x_b$. This leads to the following equation for the bond breaking speed:

$$v = \omega_0 \cdot x_b \cdot \exp\left(-\frac{(E_b - f \cdot x_b)}{k_b \cdot T}\right). \quad (2)$$

This equation can be rewritten in the following way:

$$v = v_0 \cdot \exp\left(\frac{f \cdot x_b}{k_b \cdot T}\right), \quad (3)$$

with v_0 as the natural bond breaking speed (when no load is applied), defined as:

$$v_0 = \omega_0 \cdot x_b \cdot \exp\left(-\frac{E_b}{k_b \cdot T}\right). \quad (4)$$

This modified framework enables us to study the dependence between the unfolding force and the bond breaking speed or to calculate the force at which a bond breaks, at a certain pulling rate. We can rewrite Eq. 3 in the following way:

$$f(v) = \frac{k_b \cdot T}{x_b} \cdot \ln v - \frac{k_b \cdot T}{x_b} \cdot \ln v_0 = a \cdot \ln v + b, \quad (5)$$

where $a = k_b \cdot T/x_b$and $b = -k_b \cdot T/x_b \cdot \ln v_0$. Equation 5 predicts that the unfolding force depends logarithmically on the pulling speed. We note that it contains two parameters a and b, which can be calculated exactly from the parameters x_b and E_b for a certain temperature.

Equation 5 now provides an immediate link between the pulling rate and the pulling force that is necessary to lover the energy barrier in such a way that the bond can be broken with the applied velocity; increasing the pulling rate means increasing the probability of bond rupture. This is due to lowering of the energy barrier at the transition point, because of the applied force f. We emphasize that typically several unfolding mechanisms exist, each of which is characterized uniquely by the pair x_b and E_b.

We note that multi-transition state energy landscapes were already predicted in [37]. However, the driving parameter in the theory discussed in [37] was the loading rate (the increase in force over time), and not the pulling rate as done here.

A strategy to determine the dependence of the unfolding force f on pulling speed, associated mechanisms and energy barriers is to use atomistic modeling, as described in the following sections.

Atomistic modeling methods

Atomistic modeling

Here we employ atomistic simulation to provide a bridge between microscopic length- and time scales such as quantum chemistry, and macroscopic scales such as continuum mechanics. We use classical molecular dynamics (MD).

Our MD simulations are carried out with the program NAMD [42] using the CHARMM22 force field [43]. The CMARMM22 force field is a reasonable model for atomistic interactions within proteins and between different proteins (including covalent bonds, H-bonds, electrostatic interactions and vdW interactions).

To apply the forces to the molecule that induce deformation, we use steered molecular dynamics (SMD) [42]. To apply load, C_α atoms at one end are fixed and the force is applied on the C_α atom at the other end. The SMD technique is equivalent to attaching one end of a virtual harmonic spring to the end of the system and pulling at the virtual atom on the other end of the spring [16]. The SMD method thus mimics an experiment where one end of the molecule is fixed (e.g. on a gold surface), while the other end is pulled at with the AFM cantilever tip. Using this technique, different loading conditions (e.g. tensile and bending) can be realized.

The force experienced by the virtual atom is given by [16]:

$$F = k(v \cdot t - x). \quad (6)$$

Here, x is the displacement of the pulled atom, v the pulling velocity, t the time step, and k is the spring constant.

For the tensile loading simulations described in this paper, the SMD spring constant is k = 10 kcal/mol/Å^2. Different pulling rates (v) used for the simulations are indicated in the corresponding sections.

In the bending simulations, we chose a fixed pulling rate v = 0.000,002 Å/fs, with a spring constant k = 0.01 kcal/mol/Å^2.

By monitoring the applied force (F) and the position of the atom that is pulled (x) over the simulation time, we obtain force-versus-displacement data that is used to derive the mechanical properties such as bending stiffness or the Young's modulus [44].

Molecular strain is defined as $e = (x - x_0)/x_0$, where x_0 is the initial, undeformed length, and x is the current, deformed length of the protein structure.

Due to the time scale limitations of MD to several nanoseconds, there is typically a huge difference between simulation and experiment with respect to pulling rates. Experimental rates are six to eight magnitudes smaller than in MD simulations, which requires additional consideration in order to interpret MD results in light of experimental findings.

Tensile and bending simulations were performed at a temperature of 300 K (*NVT* ensemble), with temperature control using a Berendsen thermostat. The time step used in all atomistic simulations discussed in this article is 1 fs.

We use Visual Molecular Dynamics (VMD) for visualization of protein structures [45].

Initial protein structures

We take structures obtained from X-ray diffraction experiments and stored in the Protein Data Bank (PDB) as the starting point for our atomistic simulations.

The first structure taken from the PDB is a 52 residue long coiled-coil from the 2B segment (residues 355-406; PDB ID 1GK6). The second structure is a single alpha helix from the same coiled-coil. To obtain the geometry of a single alpha helix, we extract one of the helices from the 1GK6 PDB file. Hydrogen atoms and charges are assigned according to pH 7.

The coiled-coil part considered in this paper is colored in yellow, as shown in Fig. 1a. The structure obtained from the PDB is solved completely in a water skin that encompasses the entire protein.

We perform energy minimization and finite temperature equilibration of all structures simulated before the protein is loaded by applying the SMD technique.

Computational results

Tensile deformation of single AHs and coiled-coils

Figure 4a shows the loading case for both structures considered. Figure 4b depicts the force versus strain response of a single AH and the coiled-coil structure, both carried out at identical loading rates of 5 m/s. We note that the force in Fig. 4b is normalized by the number of AHs in the structure (that is, one for the single AH, and two for the coiled-coil).

For both cases, we observe three distinct regimes (I–III) characterizing the stretching dynamics of the protein. These three regimes are now characterized first for the coiled-coil structure before the differences between the single AH and the coiled-coil are described.

In the first regime (I), the helical structure is stretched homogeneously. At the angular point (indicated as ''AP'' in Fig. 4, and marked with ''**x**'' in the plot), the structure begins to unfold by rupture of H-bonds, characterized by a significant change in slope in the force–strain plot, leading to regime (II). The AP thus represents the critical force necessary to induce a structural change in the protein, corresponding to the unfolding force.

We observe that unfolding is initiated at the end where the load is applied. In the case of the coiled-coil, each of the two alpha helices unfolds individually, while the secondary superhelical arrangement remains intact, until strains reach more than 100%. Unfolding of each AH structure is characterized by sequential breaking of H-bonds. During this regime, the force remains approximately constant while the entire protein is unfolded at strains approaching 150%.

Once the complete helix is unfolded, the slope increases continuously while the secondary superhelical configuration is lost at strains larger than approximately 150%, eventually leading to stretching of covalent bonds in the

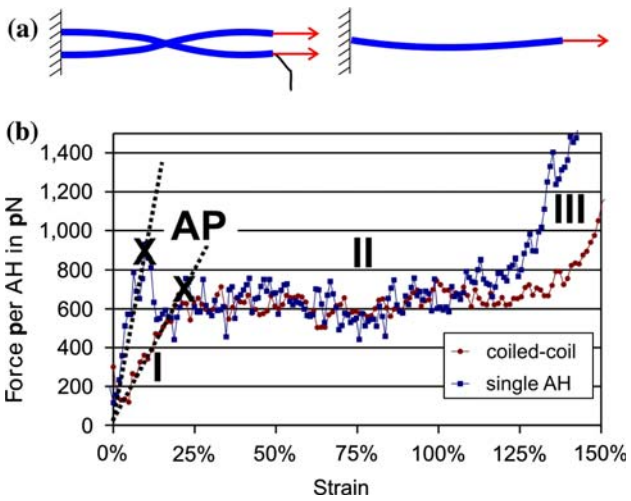

Fig. 4 Tensile experiments of vimentin proteins. Subplot (**a**) depicts a schematic of the applied load (left: coiled-coil, right: single AH). Subplot (**b**): The force–strain curves of a single AH-structure and an alpha-helical coiled-coil, both at a pulling rate of 5 m/s. To enable better comparison of both curves, the force of the coiled-coil is divided by the number of helices. The first regime (I) consists of a steep increase in force until a strain of approximately 25% (referred to as angular point (AP)) for the coiled-coil and 13% for the single AH. The first regime is followed by the second regime (II) during which unfolding of the alpha-helices occurs. The forces at the AP are much higher for a single AH than for the coiled-coil. In the third regime (III), a non-linear increase in strain by stretching the backbone is observed. Thereby the single AH has a much steeper and earlier increase in force than the coiled-coil structure. The differences between the single AH and the coiled-coil structure are summarized in Table 3

protein backbone, giving rise to rapidly increasing forces at large deformation in regime (III).

This unfolding sequence (first unfolding of individual AHs, then unfolding of the superhelical structure) suggests that in the coiled-coil case, the individual AHs represent the weakest link in the structure.

Figure 5a and b depict snapshots of the AH coiled-coil and the single AH during the three regimes.

Even though the unfolding curves of single AHs and coiled coil structures are qualitatively similar, there are several significant quantitative differences.

First, the slope of the single AH in the first regime is almost two times steeper and leads to much higher forces at the angular point. The angular point appears at strains of 13% in the single AH structure, compared with 25% for the coiled-coil. Second, unfolding of the single AH begins at the residue where the pulling force is applied, but is followed by immediate additional rupture of H-bonds at residue 369 and 383 inside the protein. Third, strain hardening of the single AH sets in at 20% lower strains; 125% in the single AH case versus 145% in the coiled coil. The strain hardening increases much steeper in the case of a single AH. The reason for this difference is likely due to the uncoiling process of the superhelical structure that is missing in the pure AH structure. The differences between the two structures are summarized in Table 3.

To investigate the pulling rate dependence of vimentin mechanics, we have carried out pulling experiments with systematically varying pulling rates. Figure 6 depicts force–strain curves for different pulling velocities, clearly illustrating a strong pulling velocity (or, equivalently strain rate) dependence of the mechanics of AH coiled-coils. We find that the force–strain curves show a significant dependence on the pulling velocity. Increases in the pulling velocity lead to increased slopes in particular in regimes (I) and (II).

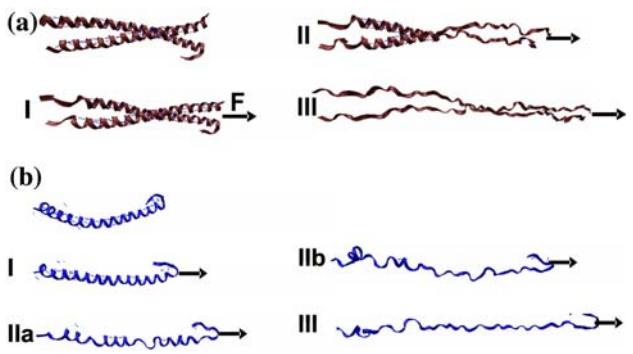

Fig. 5 Snapshots of the structures during different regimes under tensile loading (pulling rate of 5 m/s in all cases). Subplot (**a**): Snapshots of a coiled-coil during three regimes (regime (I): homogeneous stretching, regime (II): propagation of unfolding wave, regime (III): uncoiling of superhelical structure and stretching of protein backbone). Subplot (**b**): Snapshots of a single AH structure as it undergoes unfolding. The coiled-coil unfolds systematically starting at the point, where force is applied. The H-bonds of the single AH structure rupture at several convolutions simultaneously (IIa), which seem to be chosen randomly and is followed by unsystematic unfolding

Table 3 Comparison of the mechanics of single AH with the coiled-coil in different dimensions. The data were derived from simulations with a pulling rate of 5 m/s. It clearly indicates that the single AH has much more irregularities and instabilities compared to the coiled-coil, suggesting a higher mechanical stability of the coiled-coil structure

Dimension	Single AH	Coiled-coil
Equilibrated H-bond length in Å	3.08 ± 0.29	2.97 ± 0.16
Slope of the first regime in pN/Å	186.1	94.9
Force per AH at angular point in pN	930	670
Strain at angular point	13%	20%
Breaking of H-bonds	Simultaneous	Sequential
Beginning strain hardening at	125%	145%
Strain hardening	Very steep	Continuous

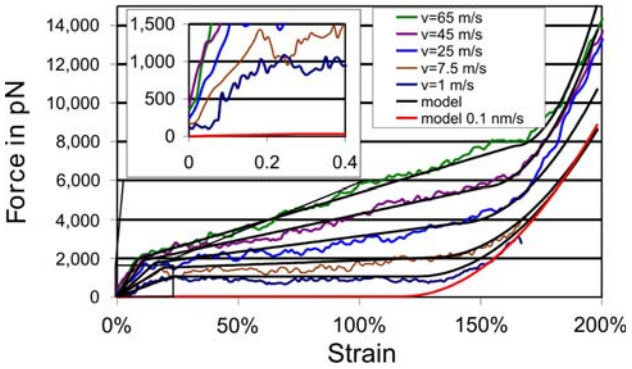

Fig. 6 Force–strain curves of a coiled-coil alpha-helical structure at different pulling rates. We describe the behavior with the developed continuum model and extrapolate to pulling rates, used AFM experiments. For pulling velocities of smaller than 5 m/s the strains, where the regime changes take place are very similar to those found in experiments and are 20% for the angular point and 120% for the beginning of the strain hardening. The straight lines refer to the prediction of our continuum model, for various pulling rates

In the following sections, we report a detailed analysis of the different deformation regimes, linking atomistic process with the observed force–strain responses.

First regime (I): stretching of H-bonds

In order to understand the deformation mechanisms and associated driving forces during the first regime, we analyze the behavior and the length of the H-bonds as the applied force is increased continuously.

The first regime is characterized by homogeneous, elastic stretching of the entire structure, where the elastic

strains are contributed largely from stretching of H-bonds in the AH arrangements.

Figure 7 depicts the average length of H-bonds, for different end displacements, for the case of a pulling rate of 5 m/s (results shown only for the coiled-coil structure). We find that the H-bonds have an initial average length of 2.97 Å, and show a rather homogeneous length distribution over the entire sequence. As the lateral loading is increased, the H-bonds are being stretched until unfolding is initiated at displacements between 14 Å and 20 Å. Unfolding occurs highly localized at the ends of the protein structure.

Under typical large MD pulling rates, most H-bonds in the protein are never stretched close to their rupture distance since the localized unfolding mechanism is activated. However, we observe that the slower the pulling rates, the more homogeneous the strain distribution at the onset of unfolding.

Second regime (II): protein unfolding

The second regime starting at the angular point (AP) is dominated by unfolding of individual AHs due to the continuous rupture of H-bonds.

Figure 8 depicts the length of the H-bonds of all residues at different displacements, for the coiled coil geometry (Fig. 8a) and the single AH structure (Fig. 8b). In both cases, unfolding initiates by significant stretching of H-bonds at both ends of the proteins where the structure is either fixed or the pulling load is applied.

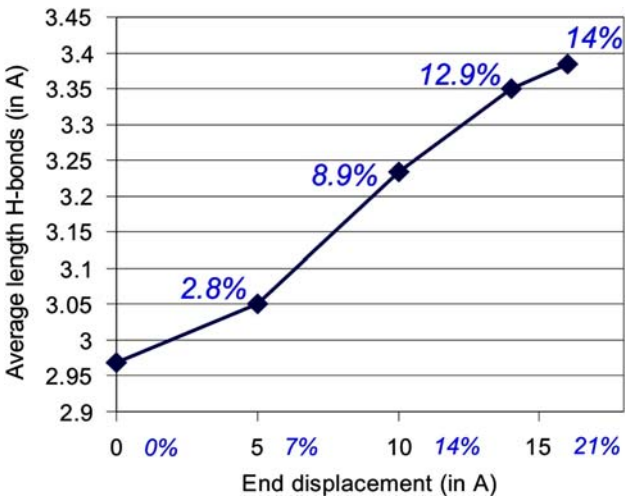

Fig. 7 Average length of H-bonds in the coiled-coil vimentin protein. As the loading is applied, the H-bonds in the protein are stretched increasingly, resulting in an increase of the average distance of H-bonds. Unfolding initiates at the end of the protein when the lateral end displacements reaches 14 Å. The italic labels at the *x*-axis indicate the molecular strain; the italic labels inside the plot correspond to the H-bond strain. Apparently, the average H-bond strain is always smaller than the molecular strain

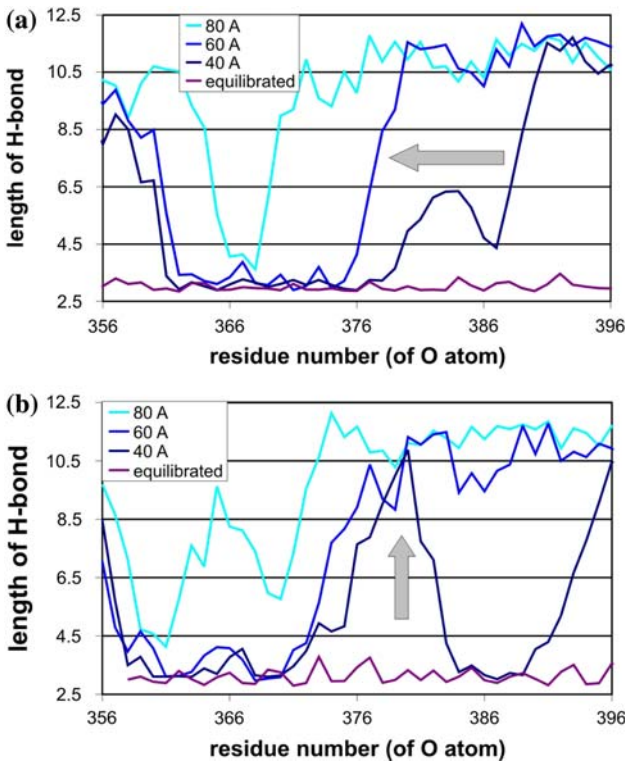

Fig. 8 The H-bond rupture dominates the second regime (data from simulation with v = 1 m/s). Once the H-bond is broken, the convolution unfolds to a length of approximately 11 Å. Subplot (**a**) shows the results for the coiled-coil structure. A rupture-wave moving away from the point of applied force can be observed. Subplot (**b**): Results for the single AH structure. Here, beside the boundary effects at both ends, rupture starts at residue 381, and is propagating first into the direction, where load is applied and afterwards in the opposite direction, indicating a more random process. No clear unfolding wave is observed in this case

Unfolding of the coiled-coil (Fig. 8a) can be characterized by an unfolding wave that starts at the end where the load is applied. The unfolding wave represents propagation of the unfolding front running through the entire protein structure (from the right to the left in Fig. 8a).

In contrast to the coiled-coil structure, unfolding of the single AH is less systematic (Fig. 8b). It begins with rupture of H-bonds at residue 381, which is approximately in the middle of the structure. This effect occurs at random residues that vary from simulation to simulation.

In order to quantify the speed of the unfolding wave, in Fig. 9a we plot the position of the H-bond in the equilibrated protein at the moment of rupture (defined for an H-bond length of more than 5 Å), for various pulling rates. We define the speed of the unfolding wave as the slope of this curve, which is determined by fitting a linear function. Figure 9b plots this unfolding wave speed as a function of pulling velocities. The dependence of the unfolding wave speed on the pulling speed is almost perfectly linear.

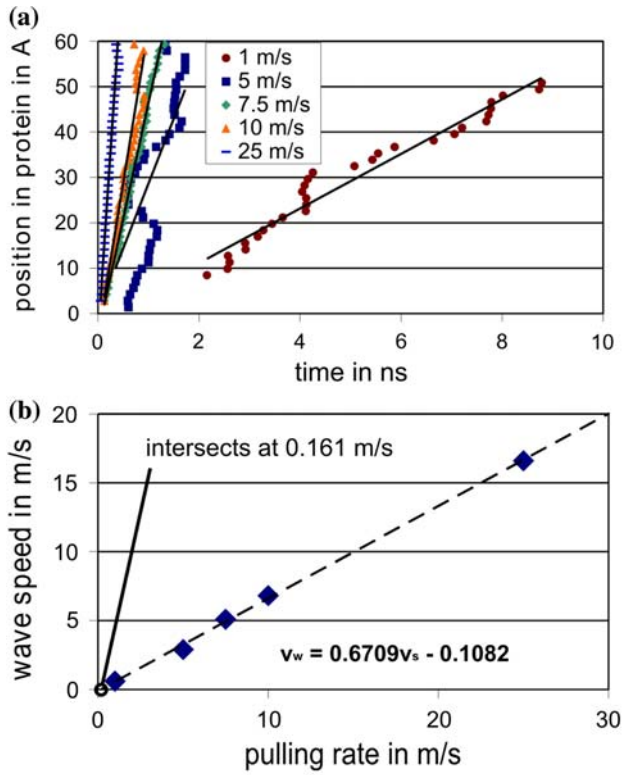

Fig. 9 Subplot (**a**): The position of the rupturing H-bond is plotted over the time. For simple calculation of the wave speed, we defined the point where pulling load is applied as 0 Å. The rupture wave propagates originating from this point in a very systematic order. We defined the slope of the linearly fitted function as the wave speed. Subplot (**b**): The wave speed equals to the slope of the linear fits in subplot (**a**). In subplot (**b**) we plot the wave speed as a function of the pulling rate. A linear function fits the relations in a excellent manner. The wave speed is of about 67% of the pulling speed, what indicates, that the pulling is much faster than the unfolding. Furthermore, we found the intersection of the linear fit and the *x*-axis at a pulling rate of 0.161 m/s

We find that the unfolding wave speed equals to 67% of the pulling speed, indicating that the unfolding is approximately 33% slower than the pulling speed. Additionally, we observe that the linear curve intersects the zero line of the horizontal axes at a pulling velocity of 0.161 m/s. This means that the deformation wave vanishes at this pulling speed of $v_{cr} = 0.161$ m/s.

Vanishing of the unfolding wave at this pulling speed has an important consequence for the unfolding mechanism. For pulling rates $v > v_{cr}$, unfolding is initiated by localized destruction of the helical structure, while strains in the other parts of the protein remain relatively low. At slower rates, strain distribution becomes more homogeneous and larger over the entire protein sequence.

Therefore, when $v > v_{cr}$, all H-bonds in the coiled-coil are strained homogeneously, and rupture occurs at a random location rather than at the location where the force is applied, representing a different unfolding mechanism. We will discuss this mechanism in 'Pulling rate dependence: change in mechanism'.

Third regime (III): unfolding of the coiled-coil structure and stretching of protein backbone

In regime (III), a non-linear increase in strain by stretching the backbone is observed, reaching forces on the order of several nN at strains approaching 200%.

Figure 10 plots some snapshots of the unfolding processes (for the coiled-coil geometry), indicating that the amino acid backbone is not completely straight immediately after rupture of H-bonds. This suggests that the straightening of the unfolded protein happens at forces that are higher than the H-bond rupture forces. This explains the continuous and smooth increase of the stiffness during strain hardening (regime (III), Fig. 4).

We find that the single AH has a much steeper and earlier increase in force than the coiled-coil structure. This is because uncoiling of the superhelical structure is missing for the single AH structure.

In contrast to regime (I) and (II), we observe only negligible pulling rate dependence in regime (III), when

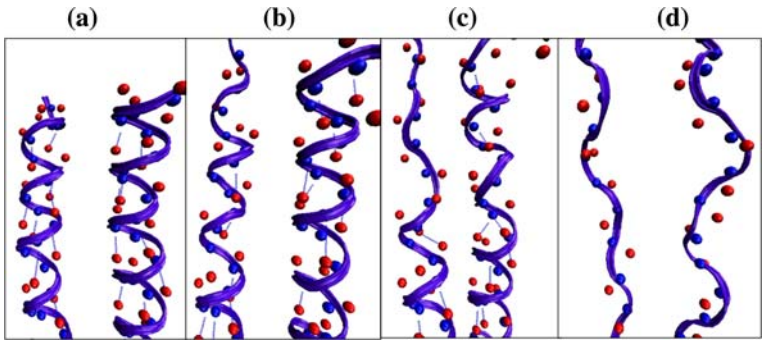

Fig. 10 Snapshots of the unfolding dynamics. Breaking of H-bonds is followed by immediate unfolding of the convolution. However, after the unfolding, the convolution is not straightened completely, which does not happen until higher forces are applied during strain hardening (regime (III)). Oxygen atoms are in red, nitrogen atoms in blue. The H-bonds are represented by the light blue lines. The direction of the pulling force is upwards

deformation is primarily characterized by stretching of covalent bonds.

Pulling rate dependence: change in mechanism

We believe there exist at least two different modes of unfolding of coiled-coil structures. The first mode is characterized by generation of a localized unfolding wave as described in detail in 'Second regime (II): protein unfolding'. We first analyze this deformation mode.

As pointed out in 'Theoretical concepts: Modified Bell theory', the accessible mechanisms and associated parameters E_b and x_b are an immediate consequence of the atomistic structure and atomic interactions. The results of MD simulations shown in Fig. 6 are now used to extract activation barrier and activation distance associated with this mode of deformation.

Figure 11 plots the results of angular point forces from simulations with varying pulling rates (data extracted from Fig. 6). In agreement with the theoretical prediction, we observe a logarithmic dependence of the force at the AP on the pulling rate.

By directly fitting the results from atomistic simulation to Eqs. 4 and 5, we obtain $E_b = 5.6$ kcal/mol and $x_b = 0.17$ Å. These values indicate that at the angular point, an individual H-bond is broken, as it is known that E_b for H-bonds is between 4 and 5 kcal/mol.

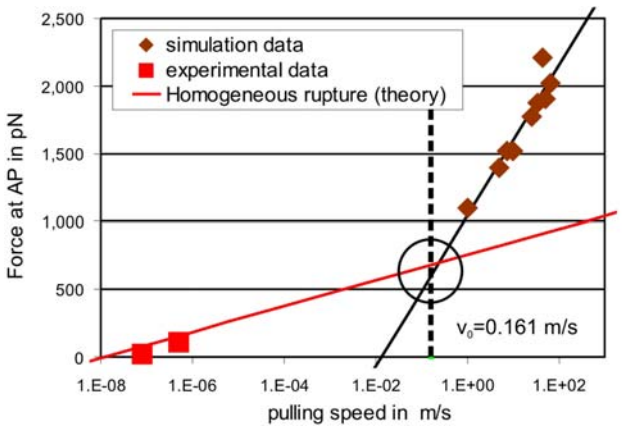

Fig. 11 Theoretical predictions for the unfolding force at the angular point (AP) compared with simulation and experiment. Simulation directly proves existence of the first mechanism (local unfolding, brown data points), with $E_b = 5.6$ kcal/mol and $x_b = 0.17$ Å (results obtained directly from fitting to the simulation data). The ''local unfolding'' mode is characterized by a deformation wave that is linearly proportional to the pulling speed (see Fig. 9). The deformation wave vanishes at a pulling speed of $v_{cr} = 0.161$ m/s (see thicker, dotted line), suggesting that below 0.161 m/s, H-bonds are strained homogeneously. This gives rise to a different deformation mode characterized by simultaneous breaking of three H-bonds (''homogeneous rupture''), so that $E_b = 15$ kcal/mol and $x_b = 1$ Å. The continuous red line indicates the theoretical prediction based on this theory. Experimental results [6, 29] agree well with the theoretical prediction

This mechanisms ceases to operate when $v > v_{cr}$, due to disappearance of the unfolding wave. The most significant consequence of the disappearance of the unfolding wave is that rather than inducing large local strains, the entire molecule is stretched homogeneously. Therefore, the H-bonds that stabilize the helical structure are strained equally under the applied load.

For rupture to occur, three H-bonds representing a complete convolution is broken simultaneously, at a random location in the coiled-coil. Assuming that a single H-bonds has a rupture energy of 5 kcal/mol with rupture distance of 1 Å, the total rupture energy is $E_b = 15$ kcal/mol and $x_b = 1$ Å. Estimates for breaking distance and energetics of breaking H-bonds are taken from the analysis reported in [46].

Figure 11 plots the force at the AP as a function of pulling speed, including the predictions for both deformation modes (continuous lines). The extended Bell theory combined with the predicted change in unfolding mode (rupture of one bond at high pulling rates versus rupture of three parallel bonds at slow pulling rates) creates a reasonable link between the very small pulling rates applied in experiments (nm/s) and several magnitudes higher velocities used in MD (m/s), and thus enables to predict the unfolding force (force at the angular point) as a function of the pulling speed.

Interestingly, the pulling speed corresponding to vanishing unfolding wave speed lies in close proximity to the intersection of the two modes of deformation (see circle in Fig. 11). This provides additional, independent prove for the change in mechanism, and suggests that the second mechanism—homogeneous rupture of three H-bonds in a convolution—is correct.

We note that these concepts also make sense from a biological point of view: Nature forms three H-bonds in parallel, instead of forming a single, much stronger bond, as three H-bonds are energetically easier to create. However, this concept only makes sense if the three H-bonds are rupturing at the same time, which indeed appears to be the case under smaller strain rates comparable to those present under physiological conditions.

Not much is known about the specific pulling velocities that appear under physiological conditions. MT are rearranged with pulling velocities in the magnitude of μm/min [47], close to pulling rates used in the experiments reported in [6, 29]. However, pulling rates sensed by the IF networks inside cells due to external load (e.g. during physical activity such as running) may lie in the regime between experiment and simulation.

Figure 12 provides an illustration of the competition between two mechanisms, each characterized by a pair of

E_b and x_b, by plotting the free energy landscape under different applied loads. When pulling is applied, the higher barrier that is further away from the equilibrium is lowered. At the point where a change in mechanism is predicted, the higher barrier becomes lower due to the applied force than the lower barrier.

Bending of single AHs and coiled-coils

In addition to the tensile tests described in 'Tensile deformation of single AHs and coiled-coils' we also perform bending simulations with the objective to calculate the bending stiffness and the persistence length of the coiled-coil dimer as well as of the single protein.

Using the double supported three-point bending test—known from engineering mechanics—as a reference model, we fix the C_α-atoms at both ends of the protein, and apply a force at the middle of our system. As a result, we obtain the force–displacement curves at the pulling point (see Fig. 13).

Taking the differential equation of a continuum Euler-Bernoulli beam (with u as the out-of-plane displacement, EI as bending stiffness, and F as the applied force)

$$EI \cdot u'''(x) = -F(x) \tag{7}$$

as a starting point and applying the boundary conditions, we receive the following expression for the bending stiffness:

$$EI = \frac{F}{d}\frac{L^3}{48}, \tag{8}$$

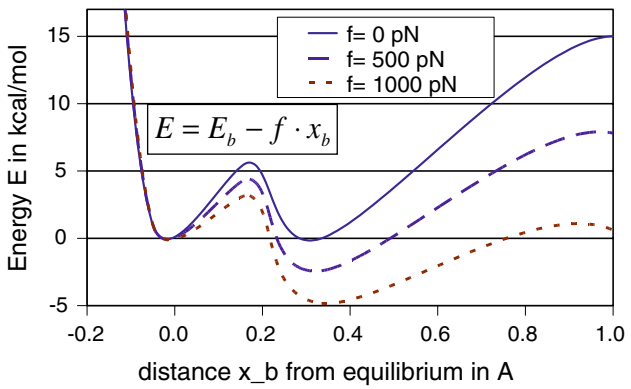

Fig. 12 Fitting Bell's theory with experimental and simulation results, we predict the following energy landscape for coiled-coil structure for different forces f at angular point. The equation indicates, how the energy is calculated. The equilibrium energy and distance is set to 0. The first transition state appears 0.17 Å away from the equilibrium, the second transition state appears at 1 Å. We can see that at forces of 700 pN or less—which we predict to appear in experiments—the second transition state is dominating. At higher force (dotted lines), the first transition state, observed in simulation has higher energies compared to the second transition state

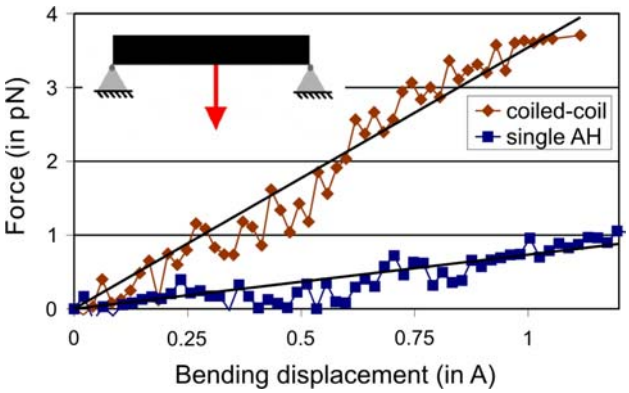

Fig. 13 Bending of a single AH and the coiled-coil, both feature a length of 71 Å. The pulling rate is 0.2 m/s. The slope of both curves, here illustrated by a linear fit is proportional to the bending stiffness, and indicates the coiled-coil to be about 4.8 times stiffer than the single AH. We used Eq. 8 for calculating the bending stiffness and derived for the coiled-coil a value of 2.60×10^{-28} Nm^2, and for the single AH 0.54×10^{-28} Nm^2. We believe that this difference is a direct consequence of the changed geometry and thus increased second momentum of area

with L as the length of the protein, in our case $L = 71$ Å, and d as the displacement at the location where the force is applied.

The bending stiffness is proportional to the ratio F/d, which is the slope from the linear fit of our simulation results.

For the coiled-coil structure, we calculate for the bending stiffness $EI = 2.60 \times 10^{-28}$ Nm^2, and for the single AH protein, $EI = 0.54 \times 10^{-28}$ Nm^2.

Consequently, the coiled-coil is approximately 4.8 times stiffer and has therefore a much higher persistence length than the single protein. This relation is reasonable and can be attributed to the change in the area moment of inertia. If we assume that the single AH has a circular area, the change factor of 4.8 would equal to an increase in radius of about 50%, which is close to the geometrical change in going from single AH to coiled-coil geometry.

With this result, the persistence length can be estimated using the following expression:

$$\xi_P = \frac{EI}{k_B T}, \tag{9}$$

where k_B is the Boltzmann constant and T the absolute temperature in Kelvin (K). We estimate a persistence length of 63 nm for the coiled-coil and of 13 nm for the single helix.

However, it was reported that the persistence length of AHs is approximately 1 nm [48] and thus about one magnitude smaller. We explain the difference between experiment and simulation by the strain rate dependence, which was already found for tensile loads and was also

reported for bending deformation of tropocollagen molecules [49]. We address the detailed analysis of this dependence in future work.

Atomistically informed continuum model

Based on the simulation data for varying pulling rates and the analysis based on Bell's theory, we generate a continuum model, consisting of linear functions for the first and the second regime and a harmonic function for the third regime.

During the first two regimes, the slope increases linearly with increasing strain rates, while in the third regime the curvature is proportional to the square of the pulling rate. As mentioned above, we find that the force at the angular points depends logarithmically on the pulling rate, following the predictions by the theoretical model.

Model formulation and parameter fitting

We use a set of empirical equations to describe the rate dependent force–extension curves based on a continuum model. All parameters in the model are determined rigorously from atomistic simulation results. The form of the equation (e.g. the dependence of AP force on pulling speed according to Eq. 5) is based on the extended Bell theory described in 'Theoretical concepts: Modified Bell theory'.

The forces in the three regimes are given by

$$F(x,v) = \begin{cases} F_1 = (F_a \cdot x)/x_a \\ F_2 = s_2 \cdot (x - x_a) + F_a \\ F_3 = s_3 \cdot (x - x_s)^2 + F_s \end{cases}, \qquad (10)$$

where $F_a = \max(c_1 \cdot \ln(v) + c_2;\ c_{12} \cdot \ln(v) + c_{13})$, $x_a = c_5 \cdot v + c_6$, and $s_2 = \max(c_7 \cdot v + c_8; 0)$are additional parameters, and v is the pulling speed (in units of Å/fs).

Further, $F_s = c_3 \cdot x_3 + c_4$, $s_3 = c_9 \cdot v^2 + c_{10} \cdot v + c_{11}$ and $x_s = \left(F_a \cdot (1 - \frac{s_2}{s_1}) - c_4\right)/(c_3 - s_2)$.

Note that F_a and x_a are the force and the displacement at the angular point, F_s and x_s are the force and the displacement at the beginning of the third regime. The parameters c_i are summarized in Table 4.

Results of this continuum model and comparison with MD simulation results are shown in Fig. 6 (the continuous lines are the predictions by the continuum model).

Example application: cyclic loading experiment of vimentin coiled-coils

The continuum model given in Eq. 10 enables us to describe the behavior of this structure even if the strain rate is varying during the stress application or cyclic loading is applied. Figure 14a shows a prediction of the force–strain curve of an experiment of cycling loading of a coiled-coil vimentin structure.

In modeling cyclic loading, we assume that the relaxation curve for the coiled-coil structure equals to the one at pulling rates in the order of nm/s (quasistatic pulling rate, in accordance with experimental observations that show refolding processes at time scales of seconds [29]). Similar results were shown in experiments of cyclic loading for the coiled-coil structure of myosin, even though different levels of assemblies were considered [29]. Our results show qualitative agreement with these experimental studies.

Figure 14b depicts the dissipation energy per loading cycle as a function of the pulling rate. This plot clearly indicates, as predicted by [4, 24], that vimentin intermediate filaments are a stress buffering protein for higher deformation rates.

Discussion and conclusion

In this article, we focused on atomistic and continuum modeling of tensile deformation of single and coiled-coil AH structures in the rod domain of a vimentin dimer (geometry see Fig. 1). We have observed the existence of strain hardening and viscoelasticity, phenomena that have previously been known to exist at the filament level [4]. Our work confirms that these also exist at the molecular, dimer level.

Through systematic comparison of a single AH with a coiled-coil structure, we explored differences in the nanomechanical behavior of AH structures due to the first level of hierarchical assembly. We find that the less steep increase in force during the first and third regime, and the lower strain at the angular point are consequences of the superhelical structure. We find that the third regime of the coiled-coil features a smoother and less steep strain hardening, since uncoiling of the coiled-coil structure appears in addition to the stretching of the backbone. Some of the differences between AH structures and coiled-coils are summarized in Table 3.

We also have observed that the unfolding of the single AH structure at large pulling velocities is much less controlled, leading to simultaneous rupture of H-bonds at several residues at the angular point (AP), in contrast to the force–strain curve of the coiled-coil structure, where a systematic unfolding appears by propagation of an unfolding wave.

We thus conclude that coiled-coils are mechanically more stable than single AH structures. This is exemplified by the smooth change from the first to the second regime at the AP, the continuous unfolding during the second regime and the less steep increase in force during the third regime. This could also explain why such structures appear in cells

Table 4 Parameters of the continuum model derived from the curve fitting to match atomistic results within a hierarchical multi-scale scheme

Numerical parameters and its units												
c_1	c_2	c_3	c_4	C_5	c_6	c_7	c_8	c_9	c_{10}	c_{11}	c_{12}	c_{13}
220	3.60	237	–19.66	–57.71	17.40	173.52	–6.3	2.4E7	–4.55	2.7	41	1.17
pN	pN	pN/Å	pN	Å	Å	pN·fs/Å^2	pN/A	pN·fs^2/Å^3	pN·fs/Å^2	pN/Å	pN	pN

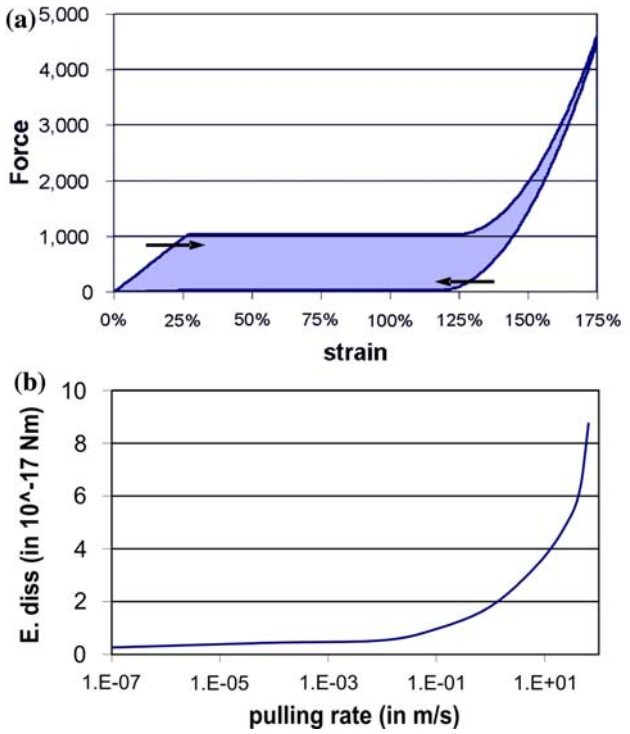

Fig. 14 Subplot (**a**): Using our continuum model, we predict the following behavior for a cyclic load experiment. In this example, we are pulling with a speed of 1 m/s. For relaxation, we assume the same behavior as for pulling with a speed of 10 nm/s. The blue area equals to the dissipated energy. Subplot (**b**): Our continuum model enables us to model the dissipation energy for the coiled-coil structure as a function of the pulling rate. The dissipation energy grows rather slowly until pulling rates of 0.1 m/s, and increases almost linearly with increasing pulling velocities afterwards (here exponential, due to the log-plot). This indicates that vimentin has strain buffering properties in cells, as it features small energy dissipation rates for small pulling rates (e.g. during cell motility), but extremely large dissipation for large pulling rates

(e.g. IFs) and tissues (e.g. muscle myosin), where high and continuously changing loads occur [1].

We have analyzed the pulling rate dependence of the coiled-coil, and developed a continuum model that enables us to predict the force–strain curves for variations in strain rates. This model is valid for pulling rates over ten orders of magnitudes, and can thus be used to calculate the behavior of vimentin proteins at pulling rates used in experiments (see Fig. 6) as well as its behavior due to cyclic loading (Fig. 14). To the best of our knowledge, this is the first atomistically informed continuum model capable of describing the nanomechanical properties of vimentin coiled-coil proteins over several magnitudes of pulling rates.

The study reported in this article illustrates how MD can be used to analyze the complex deformation mechanism in a structural protein material, overcoming some of the time scale limitations of classical MD (Fig. 11). The strategy of carrying out simulations at varying rates and interpretation of results within the framework of Bell's theory proved to be a fruitful combination that elucidates nanomechanical behavior of such structures.

Based on the atomistic simulation results, we propose a change in mechanism that occurs at pulling velocities $v_{cr} = 0.161$ m/s (Fig. 11). However, even though the change in mechanism leads to modifications in the unfolding mechanism, we find that the strain at the angular point is not influenced, since in both simulation and experiment the strain is found to be approximately 20% [29].

We have observed that the boundary conditions can play a key role in the unfolding behavior under large pulling velocities, as the H-bonds ruptures first at the fixed and the end at which the pulling force is applied. This is observed even if the fixed and pulled atoms are several convolutions away from the protein ends. This suggests that the linkers between the coiled-coils in dimers, being the ''flexible'' boundaries of the coiled-coils, might change the unfolding behavior and enable the coiled-coils to withstand higher forces before unfolding appears. This would give the linker a specific mechanical role in the dimer, and may change the energy landscape in particular at large pulling velocities. We may explore these aspects in future studies.

Our studies illustrate how Nature realizes superelasticity in vimentin coiled-coils and demonstrate that stress buffering—already known from larger scale IF networks—is also implemented at the molecular level of individual proteins.

Linking results to the filament level

Until now, few experimental results about the mechanical properties of IFs at the filament level are available. AFM studies were carried out recently for pulling desmin dimers from the surface of a filament [6], and for performing bending tests on 300 nm long filaments [26]. Additionally, AFM cantilevers were moved perpendicular to the filament axis in order to analyze the stretching and the rupture

behavior of IFs [24]. Glass micro-beam force transducer apparatus were used to measure tensile properties of single keratin IF from hagfish threads [19, 20].

In recent experiments [12], filaments were manipulated with the AFM cantilever perpendicular to the filament axis with forces between 30–40 nN and velocities of 0.4 μm/s. It was found that the breaking extension at the rupture point is up to 3.6 times of the initial length and the average extension over all experiments was 2.6 (160% strain). Assuming that there are 16 dimers in one filament, the applied force per dimer in this experiment was of about 1,800–2,500 pN.

By fitting these forces and velocities in our continuum model, we estimate protein strains of 150–160%. At this strain, the coiled-coil structure is in the third regime (the regime of strain hardening), but still far away from rupturing. The strength of covalent peptide bonds was reported to be in the order of 8 nN (and 16 nN for the coiled-coil [50]). Therefore, in addition to the protein extension, slip between proteins may occur, which may lead to additional strains of up to 50%. We derived this number by taking the length of a tetramer (approximately 60 nm; two dimer, half staggered overlap) and by assuming that after slip has taken place, the dimers are arranged sequentially, leading to a maximal length of 90 nm (two times 45 nm). Relating the difference in length (30 nm) to the initial length (60 nm) we receive a strain due to slippage of 50%. Consequently, the breaking strain being the sum of stretching and slip, can be estimated to be on the order of 200%. This is in rather good agreement with experiment (160% average, and maximum of up to 260%).

We conclude that yield in vimentin filaments appears due to the slip between proteins, as it is the weakest part in the assembled system. This idea further explains the highly reduced diameter of the ruptured filaments being a result of the unfolded proteins. This suggests that both mechanisms (extension and slippage) appear during failure of IFs. Up until now this was only suggested [20, 24]. Future AFM studies could be used to determine the forces at which slip appears, which will help to understand the mechanical properties of vimentin on the filament level.

Tensile tests were recently performed on wet keratin IFs in hagfish threads [19, 20]. The curves observed in these experiments contained four regimes, whereof the first three regimes appear very similar to the regimes that we observed in our simulations. Not only the shape of the curves, but also the strains where the changes between different regimes take place fit rather closely. For example, the angular point appeared in experiment at a strain of 34% (our simulation 25%), and the beginning of the third regime was in experiment at 100% of strain (our simulation 120%).

Additionally, if we assume that each thread (diameter of 10 nm) has in average 16 dimers (a reasonable assumption based on its diameter), we can roughly calculate the average area per dimer to be 480 $Å^2$, and use this ratio for comparing Young's Modulus between our model and experiment. Our model predicts a modulus of approximately 25 MPa, which is in good agreement with experiment (10 MPa). Additionally, the second regime in experiment was demonstrated to begin with the opening of the AH (also known as the alpha to beta transition). This was also observed in the simulation at the beginning of the second regime.

Comparing our results with those from experiments, we have shown that the specific mechanical properties of vimentin IFs at least partly originate from the protein level. Among others, the particular molecular nanomechanics explains how the large extensibility known from filament rupture experiments is possible and determined the slippage between dimers as the weaker link in filaments.

Our results let us suggest that the first regime does not appear due to the entropic elasticity of the dimer head and tail, as hypothesized in [20], but due to the stretching of the H-bonds. As long as H-bonds are not broken—which happens at the angular point—deformation is completely elastic. This type of elasticity was observed in experiment and additionally supports our hypothesis.

Linking results to other coiled-coil structures

The force–strain curves observed in our simulations are similar to MD simulations carried out on different AHs and coiled-coils [30–33], as well as to previous experimental studies on other alpha-helical coiled-coil structures such as myosin [29] or desmin intermediate filaments [6], even though the force levels are much larger due to the very high pulling velocities.

Due to the similarity in the curve shape, the similar strain levels in experiment and simulation, as well as the similar force levels in simulations for different coiled-coil structures, we conclude that the secondary structure, reinforced by H-bonds is mainly responsible for the mechanical behavior during tensile deformation, as long as point mutations do not destroy the structure. It was already suggested earlier that the mechanisms underlying the mechanics of proteins are very simple, even if the number of possible amino-acid configurations is extremely high [51]. Our observations corroborate this notion.

Interpretation of results in light of biological function

The mechanical properties of metazoan cells, its rigidity at high stresses and its integrity are mainly caused by vimentin IFs. However, up to now, it was not known exactly, from which level of hierarchy the specific mechanical properties arise. In this work we have shown which mechanical properties appear on the protein level and

proved the suggestion that coiled-coils mainly contribute to the mechanical behavior, discovered on the filament level as well as on the IF network level.

We hypothesize that Nature utilizes coiled-coils as a simple construct in order to realize superelasticity in biological materials. The deformation behavior of coiled-coils is not only elastic but also contains a long plateau at constant force (Figs. 4 and 6). Thereby, the very high and reversible deformation of coiled-coils is realized by a second, stress induced phase, which equals to the rupture of the H-bonds followed by an immediate unfolding. Once the tensile load is reduced, the second phase becomes unstable, or in other word, the structure folds back to the more stable helical shape by reforming the H-bonds. This behavior is reminiscent of a shape memory alloy.

There is another twist to this feature: The second phase may be used simultaneously as the ''security belt'' of the cell, as covalent bonds rupture at forces of three magnitudes higher than H-bonds. Additionally, the transition from the plateau regime to the stretching of the covalent bonds is very smooth so that no shock waves appear that could lead to uncontrolled rupture. Therefore, coiled-coils may be considered as the elementary building blocks of IFs that enable cells to withstand dramatic loads, large deformation and very high deformation rates.

In coiled-coil structures, H-bonds are apparently not used to generate mechanically robust structures, as can be seen by the existence of regime (II) with low unfolding forces. Instead, they provide a means of enabling low-force unfolding and simple refolding into helical structures. Strength originates from the superhelical structure and from the covalent chemistry present in the protein backbone.

The hysteresis (Fig. 14) and the strong strain rate dependence (Fig. 6) provide further evidence that coiled-coils represent strain buffering elements in cells, with the possibility to dissipate great amounts of energy as it undergoes repeated stretching and relaxation cycles. At the same time, at small deformations (smaller than approximately 20%) and small pulling velocities that appear during cell movement, the resistance of the coiled-coil is completely elastic, and thus do not dissipate energy.

The comparison of our results with those from simulations and experiments on other coiled-coils, underline the important role of H-bonds as a key in the realization of the specific mechanical properties of coiled-coils. Our results suggest that Nature creates three H-bonds in parallel (three for single AHs, and six for coiled-coils, where three are present in each AH). This is energetically much easier to realize than single bonds with strength equal to three H-bonds. Our calculations predict that during pulling velocities applied in experiments, and most likely during those appearing in vivo, three parallel H-bonds break simultaneously. This clearly supports the idea of creating parallel bonds. The coiled-coil configuration reinforces the protein additionally and makes it much more stable.

Outlook

Future studies could be focused to develop a more complete understanding of vimentin dimers, the role of the head and tail domain, the reason for the different lengths of the conserved coiled-coil segments in the rod domain, and the function of the stutter. In addition, a thorough theoretical understanding of the driving forces during assembly and the interaction of assembled IFs is still missing.

Furthermore, the time and length scale, which can be realized with MD is still comparably small. In order to overcome the limitations of length and time scale, multiscale modeling techniques could be used in future work, linking the atomistic scale through mesoscale, such as coarse graining, to the continuum scale. By using such techniques, it may be possible to shed light on the different levels of hierarchies and thus contribute to the understanding of the protein mechanics of vimentin alpha-helical coiled-coils. Techniques such as nudged elastic band (NEB) may be used to determine the energetic pathway of rupturing three H-bonds simultaneously.

The combination of new theories, experimental techniques on the nano-scale in addition to modern simulation approaches, might be the key in understanding hierarchical biological materials and thus help to heal diseases or help designing new multifunctional materials such as biological actuators.

We hope that our theoretical studies could motivate new experiments on single alpha helical as well as coiled-coil proteins. In particular, experiments are needed that produce force–extension curves for systematically varying pulling rates. Such results can be used directly to elucidate energy barriers of different mechanisms, and may be used to compare quantitatively with the theoretical concepts and results reported here.

Acknowledgements TA acknowledges the support of the German National Academic Foundation and the Dr.-Juergen-Ulderup Foundation. This research was partly supported by the Army Research Office (ARO), grant number W911NF-06-1-0291, program officer Dr. Bruce LaMattina. We acknowledge fruitful discussions with Professor Harald Herrmann (University of Heidelberg, Germany) and Professor Laurent Kreplak (University of Basel, Switzerland).

References

1. Alberts B et al (2002) In: Molecular biology of the cell. Taylor & Francis
2. Strelkov SV, Herrmann H, Aebi U (2003) BioEssays 25:243
3. Burkhard P, Kammerer RA, Steinmetz MO, Bourenkov GP, Aebi U (2000) Structure 8:223

4. Herrmann H, Aebi U (2004) Annu Rev Biochem 73:749
5. Strelkov SV, Herrmann H, Geisler N, Wedig T, Zimbelmann R, Aebi U, Burkhard P (2002) EMBO J 6:1255
6. Kiss B, Karsai A, Kellermayer MSZ (2006) J Struct Biol 155:327
7. Janmey PA, Euteneuer U, Traub P, Schliwa M (1991) J Cell Biol 113:155
8. Mücke N, Wedig T, Bürer A, Marekov L, Steinert P, Langowski J, Aebi U, Herrmann H (2004) J Mol Biol 340:97
9. Smith TA, Strelkov SV, Burkhard P, Aebi U, Parry DAD (2002) J Struct Biol 137:128
10. Wilson KL, Zastrow MS, Lee KK (2001) Cell 104:647
11. Wang N, Stamenovic D (2003) J Muscle Res Cell Motil 23:535
12. Mücke N, Kreplak L, Kirmse R, Wedig T, Herrmann H, Aebi U, Langowski J (2004) J Mol Biol 355:2342
13. Helfand BT, Chang L, Goldman RD (2004) J Cell Sci 117:133
14. Smith TA, Hempstead PD, Palliser CC, Parry DAD (2003) Proteins 50:207
15. Kreplak L, Aebi U, Herrmann H (2004) Exp Cell Res 301:77
16. Strelkov SV, Schumacher J, Burkhard P, Aebi U, Herrmann H (2004) J Mol Biol 343:1067
17. Moir RD, Spann TP (2001). Cell Mol Life Sci 58:1748
18. Coulombe PA, Bousquet O, Ma L, Yamada S, Wirtz D (2000) Cell Biol 10:420
19. Fudge DS, Gosline JM (2004) Proc R Soc Lond 271:291
20. Fudge DS, Gardner KH, Forsyth VT, Riekel C Gosline JM (2003) Biophys J 85:2015
21. Eckes B, Dogic D, Colucci-Guyon E, Wang N., Maniotis A, Ingber D (1998) J Cell Sci 111:1897
22. Brown MJ, Hallam JA, Colucci-Guyon E, Shaw S (2001) J Immunol 166:6640
23. Nieminen M, Henttinen T, Merinen M, Marttila- Ichihara F, Eriksson JE, Jalkanen S (2006) Nat Cell Biol 8:156
24. Kreplak L, Bär H, Leterrier JF, Herrmann H, Aebi U (2005) J Mol Biol 354:569
25. Storm C., Pastore JJ, MacKintosh FC, Lubensky TC, Janmey PA (2005) Nature 435:191
26. Guzmán C, Jeney S, Kreplak L, Kasas S, Kulik AJ, Aebi U, Forró L (2006) J Mol Biol 360:623
27. Omary MB, Coulombe PA, Irwin McLean WH (2004) N Engl J Med 351:2087
28. Schietke R, Broehl D, Wedig T, Muecke N, Herrmann H, Magin TM (2006) Eur J Cell Biol 85:1
29. Schwaiger I, Sattler C, Hostetter D, Rief M (2002) Nat Mater 1:232
30. Akkermans RL, Warren CPB (2004) Phil Trans R Soc Lond 362:1783
31. Root DD, Yadavalli VK, Forbes JF, Wang K (2006) Biophys J 90:2852
32. Cieplak M, Hoang TX, Robbins MO (2002) Proteins: Struct Funct Genet 49:104
33. Rohs R, Etchebest C, Lavery R (1999) Biophys J 76:2760
34. Bornschloegl T, Rief M (2006) PRL 96:118102
35. Mitsui J, Nakajima K, Arakawa H, Hara M, Ikai A (2000) Biochem Biophys Res Commun 272:55
36. Hanke F, Kreuzer HJ (2006) Phys Rev 74:031909
37. Evan E, Ritchie K (1997) Biophys J 72:1541
38. Dudko OK, Hummer G, Szabo A (2006) PRL 96:108101
39. Wiita AP, Ainavarapu SRK, Huang HH, Fernandez JM (2006) PNAS 103:7222
40. Gilli P, Bertolasi V, Pretto L, Gilli G (2006) J Mol Struct 790:40
41. Bell GI (1978) Science 200:618
42. Lu H, Isralewitz B, Krammer A, Vogel V, Schulten K (1998) Biophys J 75:662
43. MacKerell AD et al (1998) J Phys Chem 102:3586
44. Courtney TH (1990) In: Mechanical behaviour of materials. McGraw-Hill
45. Humphrey W, Dalke A, Schulten K (1996) J Mol Graphs 14:33
46. Sheu SY, Yang DY, Selzle HL, Schlag EW (2003) PNAS 100:12683
47. Inoué S, Salmon ED (1995) Mol Biol Cell 6(12):1619
48. Papadopoulos P et al (2006) Biomacromolecules 7:618
49. Buehler MJ, Wand SY (in press) Entropic elasticity controls nanomechanics of single tropocollagen molecules
50. Buehler MJ (2007) J Mech Mater Struct (in print)
51. Baker D (2000) Nature 405:39